Electronic Supplementary Material (ESI) for Nanoscale.
This journal is © The Royal Society of Chemistry 2017

Electronic Supporting Information (ESI)

Gold Nanoshurikens with Uniform Sharp Tips for Chemical Sensing by Localized Surface Plasmon Resonance

Lei Zhang,[a‡] Xiao Sha,[a‡] Qikui Fan,[a] Lu Han,[c] Yadong Yin[b] and Chuanbo Gao[a]*

[a.] *Frontier Institute of Science and Technology, and State Key Laboratory of Multiphase Flow in Power Engineering, Xi'an Jiaotong University, Xi'an, Shaanxi 710054, China;*

[b.] *Department of Chemistry, University of California, Riverside, California 92521, United States;*

[c.] *School of Chemistry and Chemical Engineering, Shanghai Jiao Tong University, Shanghai 200240, China.*

[‡] *L.Z. and X.S. contributed equally to this work.*

**Correspondence: gaochuanbo@mail.xjtu.edu.cn*

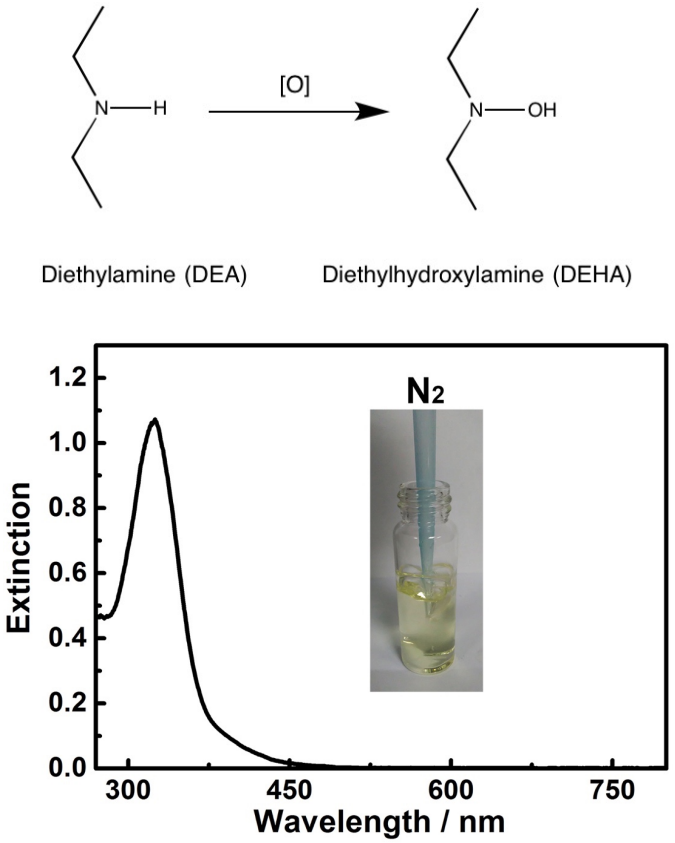

Fig. S1 Role of DEHA in the synthesis of Au nanoshurikens. Under the aerobic condition, DEA can be oxidized into DEHA, which serves as a reducing agent (a type of hydroxylamine) for the Au salt (top, a schematic reaction). When the typical reaction system was degassed by N_2, the reaction cannot be initiated (bottom, showing the color of $HAuCl_4$ instead of Au nanocrystals), which confirms the role of DEHA as a reducing agent in this synthesis system.

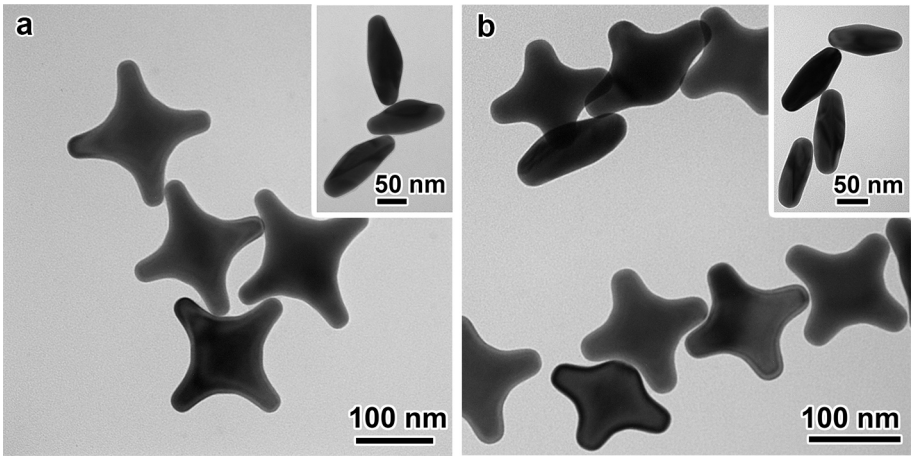

Fig. S2 TEM images of the Au nanoshurikens with blunt tips. The synthesis was conducted at 150 °C, and the reaction lengths of time were 10 min (a) and 20 min (b). It implies that with prolonged reaction time, the nanotips became much blunter due to the Ostwald Ripening.

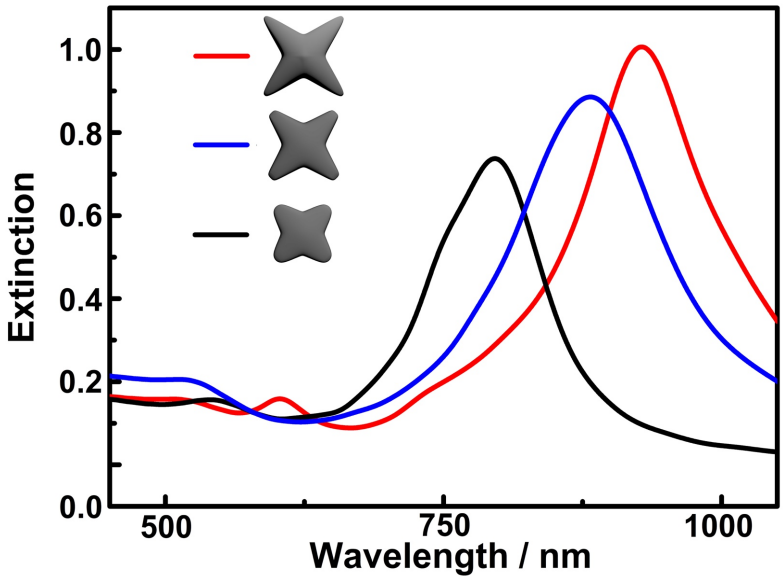

Fig. S3 Simulated UV-vis-NIR spectra of Au nanoshurikens with nanotips of different sharpness.

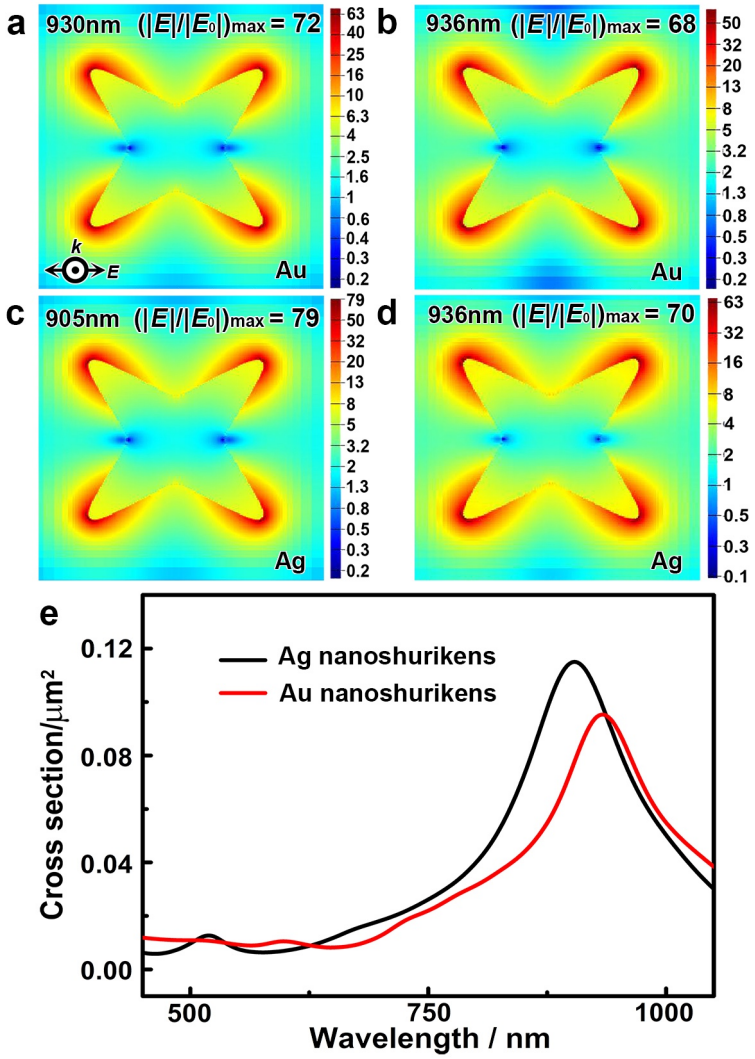

Fig. S4 Optical properties of the Au and Ag nanoshurikens simulated by FDTD. (a–d) Distributions of the electromagnetic field intensity in the proximity of the nanoshurikens, irradiated at their respective resonance wavelengths. The color bars represent the amplitude ratio of $|E|/|E_0|$, where E and E_0 are the local and incident electromagnetic fields, respectively. (e) LSPR profile of the Au nanoshurikens in comparison with that of the Ag nanoshurikens.

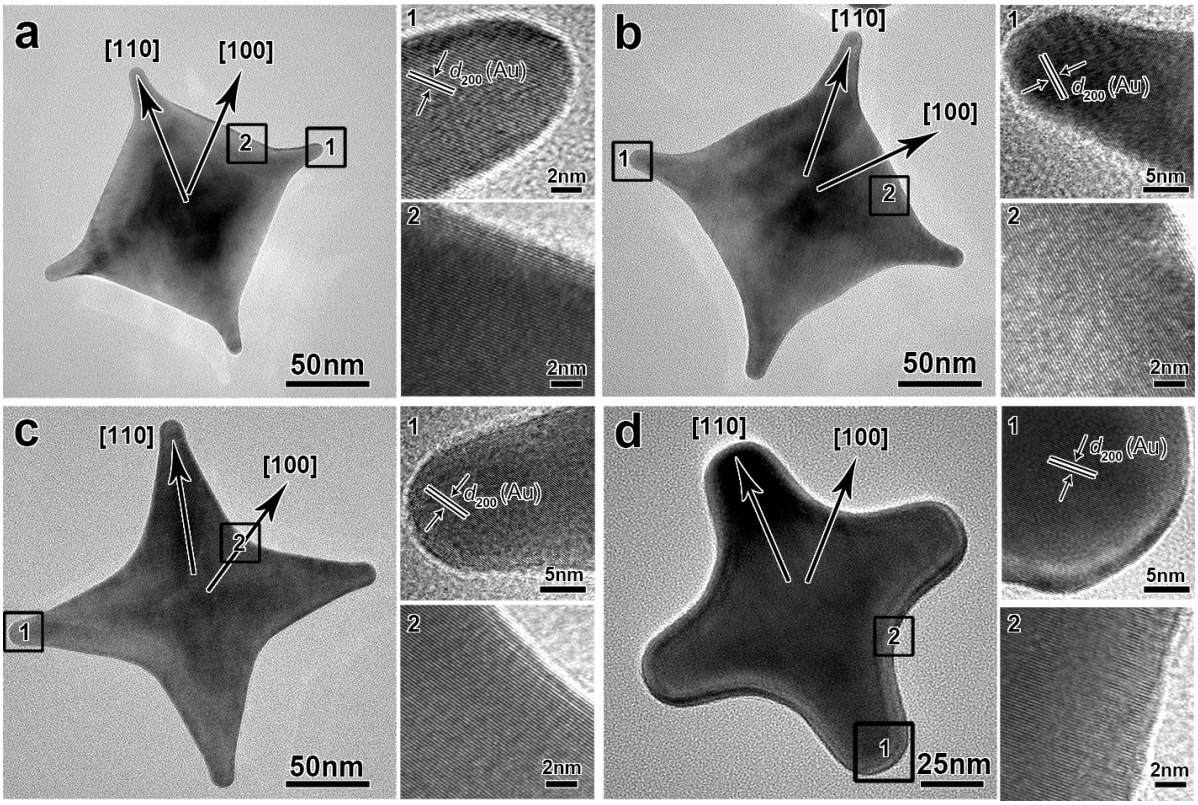

Fig. S5 HRTEM image of the individual Au nanoshurikens with different tip sharpness (corresponding to Fig. 1 a–d). It is clear that the growth of the sharp tips occurred preferentially in the [110] direction.

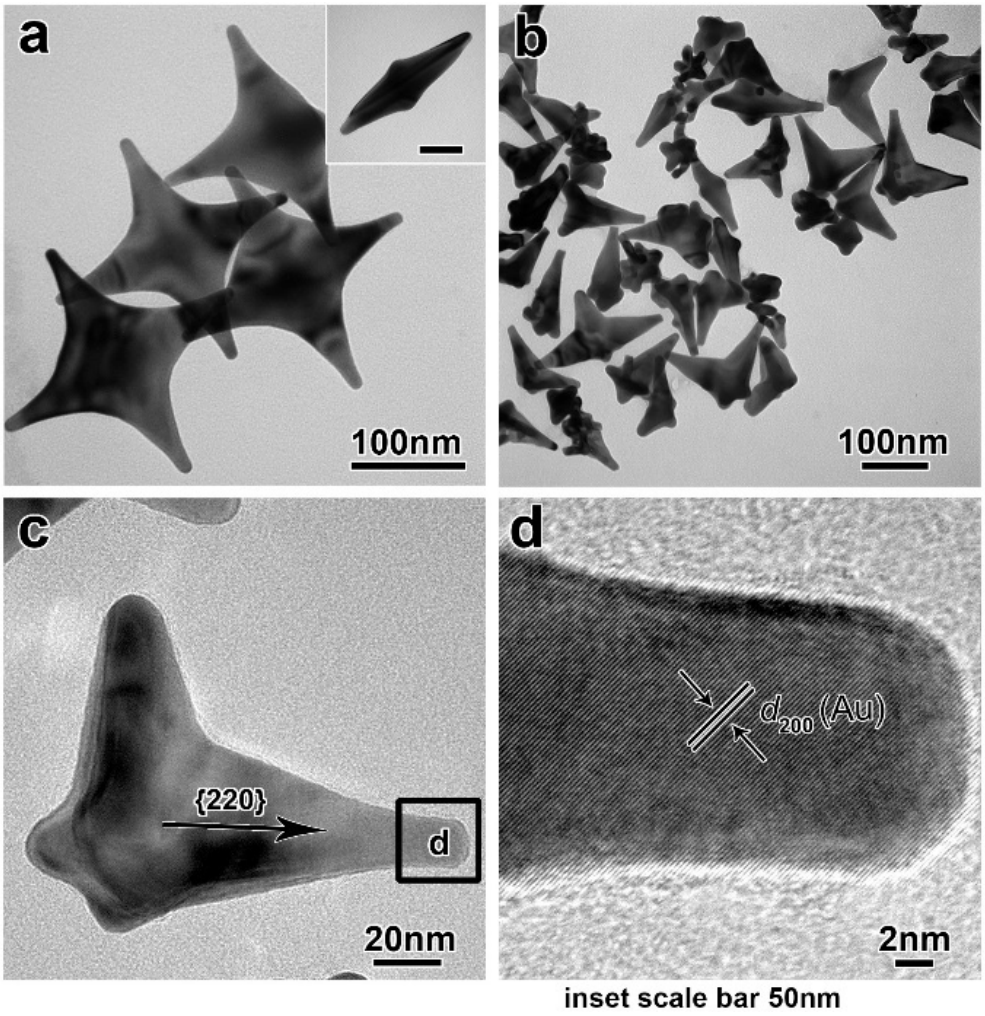

Fig. S6 TEM images of the products obtained (a) without PVP or (b–c) by using H_2O in place of DMF in a typical synthesis as described in the Experimental Section. (d) Corresponding HRTEM images of the region marked with the box in (c).

Scheme S1. Chemical Reactions during the amalgamation of Hg and Au.[1]

$$HgCl_2(aq) + 2NaBH_4(aq) + 6H_2O \rightarrow Hg(l) + 7H_2(g) + 2B(OH)_3(aq) + 2NaCl(aq)$$

$$3Au(s) + Hg(l) \rightarrow Au_3Hg(s) \quad \text{(Low Hg/Au ratio)}$$

$$Au(s) + 2Hg(l) \rightarrow AuHg_2(l) \quad \text{(High Hg/Au ratio)}$$

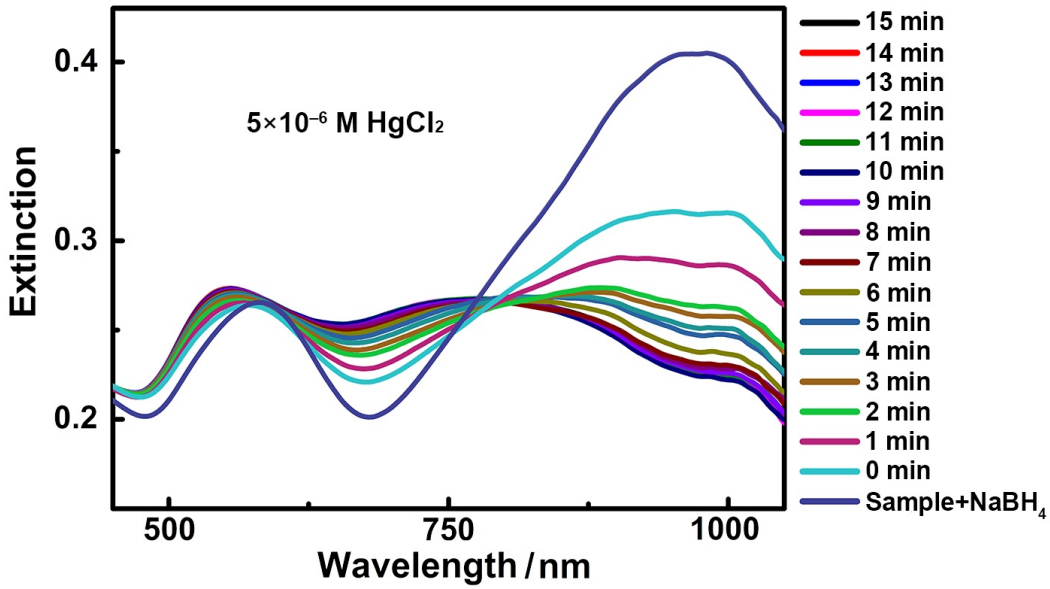

Fig. S7 UV-vis-NIR extinction spectra of the Au nanoshurikens after reaction with 5×10^{-6} M $HgCl_2$ in the presence of $NaBH_4$ at different reaction time. The extinction intensity became stable after 10 min. Thus, in all sensing experiments, the solutions were kept for 10 min before measuring the UV-vis-NIR spectrum.

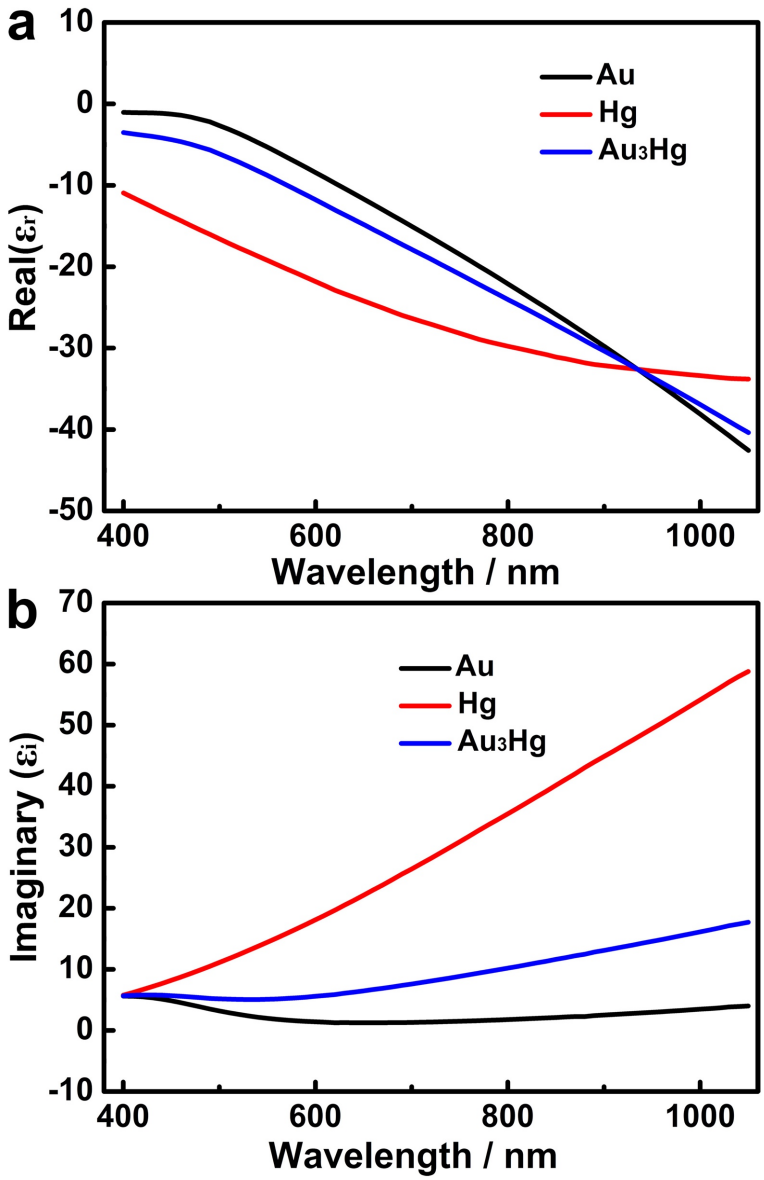

Fig. S8 Plots of the real (ε_r) and imaginary (ε_i) components of the dielectric function (ε) of Au, Hg, and Au_3Hg (by calculation) as a function of the wavelength. The complex refractive indices (n^*) of pure Au and Hg, with real and imaginary parts n and k, were adopted from the literature.[2, 3] ε_r and ε_i of pure Au and Hg can be calculated by $\varepsilon_r = n^2 – k^2$ and $\varepsilon_i = 2nk$. The dielectric constant of the alloy can be treated as a combination of ε_{Au} and ε_{Hg} in the form of $\varepsilon\ (\alpha) = (1–\alpha)\ \varepsilon_{Au} + \alpha\ \varepsilon_{Hg}$, where $\alpha = 1/4$ for Au_3Hg.[4] The plots suggest that surface modification of the Au nanoshurikens with Hg leads to a significant change in the dielectric function, which imposes strong influence on the optical property of the nanoshurikens. These values were employed for simulations of the optical property of the surface-alloyed Au nanoshurikens with Hg (Fig. 6c).

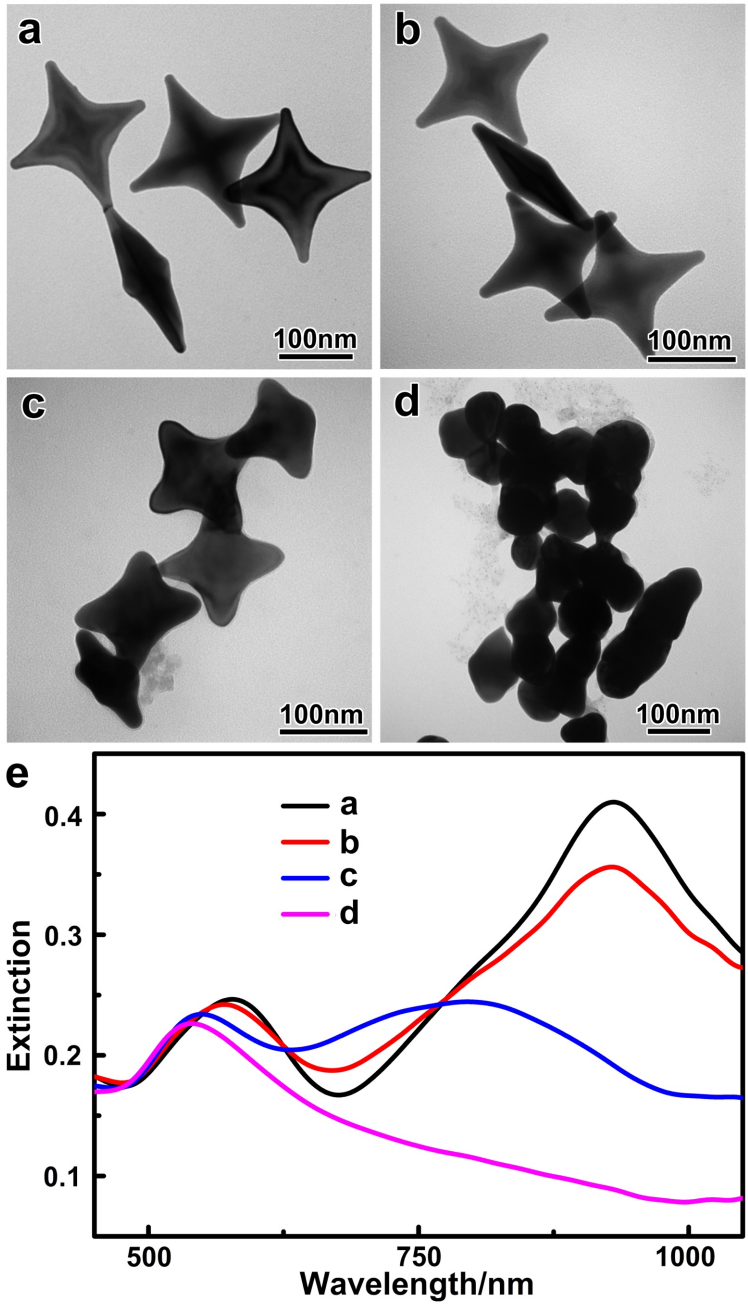

Fig. S9 (a) TEM image of the Au nanoshurikens. (b–d) TEM images of the Au nanoshurikens in the presence of $HgCl_2$ with different concentrations: (d)$_{Hg}^{2+}$ > (c)$_{Hg}^{2+}$ > (b)$_{Hg}^{2+}$. (e) Corresponding UV-vis-NIR spectra of the products.

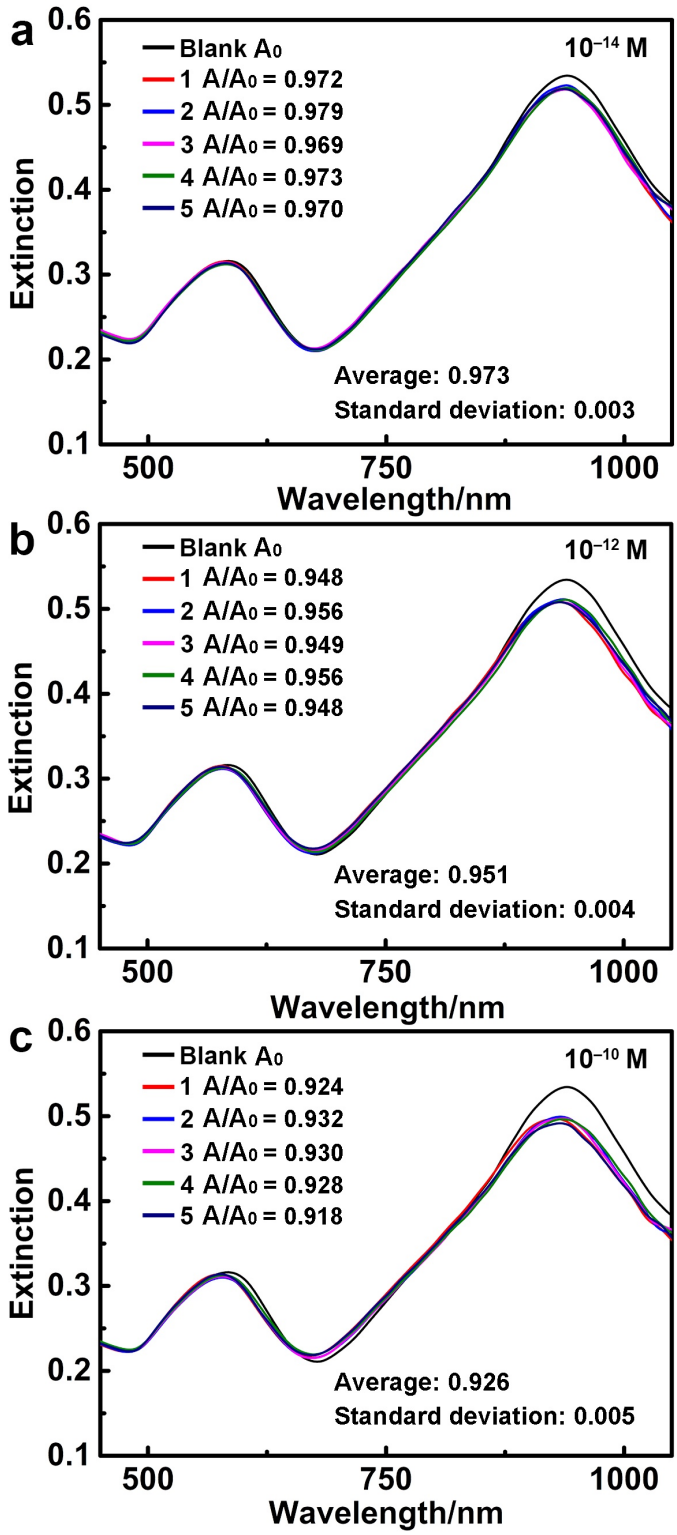

Fig. S10 Reproducibility of the LSPR-based sensing system for Hg(II) of ultralow concentrations (a, 10^{-14} M; b, 10^{-12} M; c, 10^{-10} M) by using Au nanoshurikens. For each concentration, 5 parallel analyses were conducted. It is inferred that the UV-vis-NIR spectra overlap for each concentration with very close A/A_0 values at 937 nm, with the standard deviations being only ~0.003, 0.004 and 0.005, respectively. Therefore, the sensing system can detect Hg(II) of ultralow concentrations in a very reproducible manner.

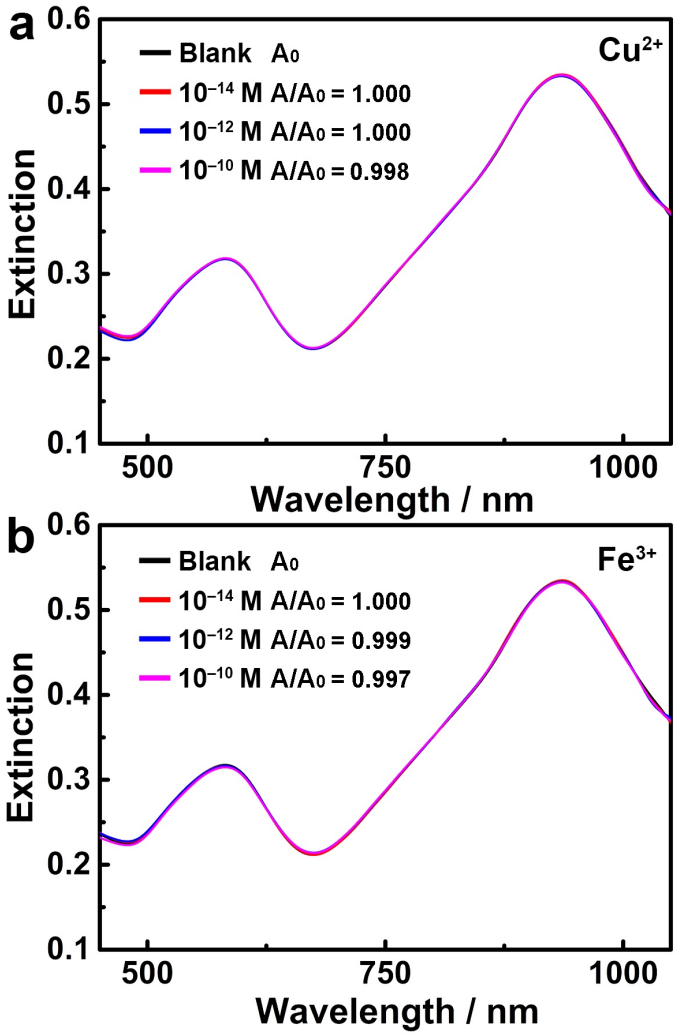

Fig. S11 The LSPR response of the sensing system toward other metal ions, Cu^{2+} (a) and Fe^{3+} (b) respectively, in comparison with Hg(II) of the same concentrations (Fig. S10). No significant change of the LSPR intensity can be detected in the presence of Cu^{2+} and Fe^{3+}, confirming the high selectivity of the sensing system toward Hg(II) with high reliability at ultralow concentrations.

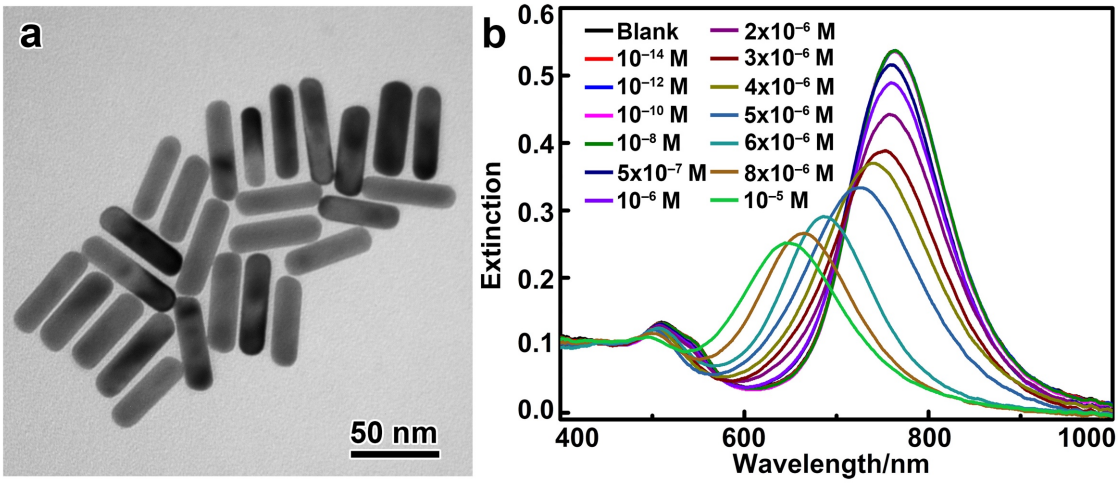

Fig. S12 LSPR-based sensing of Hg(II) with Au nanorods. The Au nanorods were synthesized according to the literature.[5] (a) TEM image of the Au nanorods. (b) UV-vis-NIR spectra of the Au nanorods in the presence of $HgCl_2$ of different concentrations (10^{-14}–10^{-5} M). The procedures of the sensing application were the same as those with Au nanoshurikens described in the Experimental Section.

Discussion on Fig. S12: When Au nanorods were used in LSPR-based sensing of Hg(II), no notable change in the intensity or band position or the LSPR can be detected in the presence of Hg(II) of low concentrations (10^{-14}–10^{-8} M). Significant changes in the LSPR property could be only observable with Hg(II) of high concentrations (> 10^{-8} M). It indicates that the sensing activity of the Au nanorods was lower than that of the Au nanoshurikens, which can be largely attributed to the greater bluntness (tip size: ~15 nm) of the Au nanorods than that of the Au nanoshurikens (tip size: ~11 nm, Fig. 1c), and therefore higher sensitivity of the LSPR in response to the change at the nanotips.

It is worth noting that other sensing systems can be found in the literature with Au nanorods, which can detect Hg(II) at a low concentration of 1.6×10^{-11} M by measuring the band shift of the LSPR. With linear assemblies of the Au nanorods, Hg(II) of an even low concentration of 10^{-13} M can be detected, which takes the advantage of significant changes in the coupling of the LSPR induced by slight variation of the Au nanorods. Compared with these results, the sensing system with the Au nanoshurikens was still superior, which can detect Hg(II) of ~10^{-14} M.

References

1. M. Rex, F. E. Hernandez and A. D. Campiglia, *Anal. Chem.*, 2006, **78**, 445-451.
2. A. D. Rakić, A. B. Djurišić, J. M. Elazar and M. L. Majewski, *Appl. Opt.*, 1998, **37**, 5271-5283.
3. T. Inagaki, E. T. Arakawa and M. W. Williams, *Phys. Rev. B*, 1981, **23**, 5246-5262.
4. S. Link and M. A. El-Sayed, *J. Phys. Chem. B*, 1999, **103**, 8410-8426.
5. X. Ye, L. Jin, H. Caglayan, J. Chen, G. Xing, C. Zheng, V. Doan-Nguyen, Y. Kang, N. Engheta, C. R. Kagan and C. B. Murray, *ACS Nano*, 2012, **6**, 2804-2817.